Journal of Materials Chemistry

Dynamic Article Links

Cite this: *J. Mater. Chem.*, 2011, **21**, 7870

www.rsc.org/materials

FEATURE ARTICLE

Polymer-stabilized optically isotropic liquid crystals for next-generation display and photonics applications

Jin Yan, Linghui Rao, Meizi Jiao, Yan Li, Hui-Chuan Cheng and Shin-Tson Wu*

Received 16th February 2011, Accepted 25th March 2011
DOI: 10.1039/c1jm10711a

Polymer-stabilized optically isotropic liquid crystals, including blue phases, are emerging as a strong contender for next-generation display technology because they exhibit some revolutionary features such as no need for surface alignment, submillisecond response time, isotropic dark state, and cell gap insensitivity. The basic material properties, including electric field-induced birefringence, dispersion relation of Kerr constant, and temperature dependent Kerr constant, are reviewed. Recent progress on blue phase liquid crystal material development and device structures for lowering the operating voltage are introduced. Promising applications and remaining technical challenges are also discussed.

1. Introduction

Blue phases (BPs) are mesophases that appear over a narrow temperature range between chiral nematic and isotropic phases. Unlike chiral nematic phases, macroscopically BPs are optically isotropic. Depending on the chirality, there are up to three types of blue phases: BPI, BPII, and BPIII, in the order of increasing temperature. While BPIII possesses the same symmetry as the isotropic phase, BPI and BPII are comprised of double twist cylinders arranged in cubic lattices,[1–4] as shown in Fig. 1(a) and 1 (c). The three-dimensional cubic structures of BPI and BPII have been validated by a number of experimental techniques,[5–7] such as selective Bragg reflections,[6] and Kossel diagrams.[7] Since double twist cylinders cannot fill the space without defects, blue phase is a coexistence of double twist cylinders and disclinations. Defects occur at the points where the cylinders are in contact, as illustrated in Fig. 1(b) and 1(d). These defects tend to make the structure less stable and, as a result, the temperature range of a blue phase is usually narrow, only 0.5–2 K. This narrow temperature range limits the applications of blue phases.

Much effort has been made to widen the temperature range of blue phase liquid crystals (BPLCs). In 1993, Kitzerow *et al.* used reactive LC monomers, which can be photo-polymerized, to form a stabilized blue phase structure.[8] However, this material does not show any dynamic switching behavior since all the molecules are polymer stabilized. In 2002, Kikuchi *et al.* reported a non-reactive BPLC stabilized by a small fraction of polymer (~8 wt%), named polymer-stabilized blue phase liquid crystal (PS-BPLC). The cross-linked polymer network is selectively concentrated in the disclination cores and the lattice structure of the blue phase is stabilized. As a result, the temperature range of

College of Optics and Photonics, University of Central Florida, Orlando, Florida, 32816, USA. Fax: +1-407-823-6880; Tel: +1-407-823-4763

Jin Yan

Jin Yan is currently a Ph.D. candidate at College of Optics and Photonics, University of Central Florida. Her research interests include device physics and materials of polymer-stabilized blue phase and isotropic phase liquid crystal displays. She has 5 journal publications in Applied Physics Letters and Optics Express. Currently, she is the vice president of SID student chapter at UCF.

Linghui Rao

Linghui Rao is currently a Ph.D. candidate at the College of Optics and Photonics, University of Central Florida. Her research interests include novel LC materials for advanced LCD applications and blue phase liquid crystal displays. She has 14 journal publications in APL, Optics Express, etc. *She is a recipient of 2010 SID distinguished student paper award and SPIE educational scholarship.*

BPLC has been extended to more than 60 K, including room temperature (260–326 K). Moreover, a fast electro-optic switching property is maintained.[9] This approach opens a new gateway for display and photonic applications.

It was also found that optically isotropic medium can be obtained even if the UV curing process was performed at an isotropic phase, where no blue phase structure is observed.[10] The electric field switching mechanism of the polymer-stabilized isotropic phase (PSIP) is similar to that of PSBP, except that the driving voltage is lower and light scattering is stronger.[11] Similarly wide temperature range (44 K) was also reported by Coles and Pivnenko in 2005.[12] The large flexoelectro-optic effect of the liquid crystal dimers was considered as the reason for the stability. This system also has potential for photonic applications since the reflected color could be switched reversibly with a response time of ~10 ms.

In this article, we will review recent progress on the optically isotropic liquid crystals, including both self-organized PSBP and PSIP nanostructured composites. For display applications, PSBP exhibits several revolutionary features: 1) it does not need any surface alignment layer, 2) its gray-to-gray level response time is in the submillisecond range,[13] 3) its dark state is isotropic so that the viewing angle is inherently wide and symmetric, and 4) its electro-optic effect is insensitive to the cell gap if in-plane switching (IPS) electrodes are employed. However, some challenges such as relatively high operating voltage, low transmittance, hysteresis, and residual birefringence, remain to be overcome before this promising technology can find widespread applications. Here, we will discuss the electric field, wavelength, and temperature effects of the optically isotropic liquid crystals.

2. Electric field effect

When a small electric field (E) is applied to a BPLC composite, the LC molecules tend to be reoriented parallel to the electric field if $\Delta\varepsilon > 0$, and perpendicular to the electric field if $\Delta\varepsilon < 0$, where $\Delta\varepsilon$ is the dielectric anisotropy of the LC. Such molecular reorientation results in a birefringence in BPLC, and the induced birefringence can be described by the Kerr effect as:

$$\Delta n_{ind} = \lambda K E^2, \quad (1)$$

where λ is the wavelength and K is the Kerr constant.[14] As the electric field increases, there are two other effects: electrostriction, which is the distortion of the cubic blue phase lattice; and a phase transition to chiral nematic phase and ultimately to the nematic phase.[5] While the Kerr effect exhibits a fast response time (<1 ms), the latter two effects are much slower, with the

Meizi Jiao

Meizi Jiao is currently an optical engineer at Apple, Inc. She received her Ph.D. from the College of Optics and Photonics, University of Central Florida, in 2010. She is a recipient of 2009 IEEE/Photonics Society graduate student fellowship award, 2009 J. SID outstanding student paper of the year award, and 2008 SPIE educational scholarship.

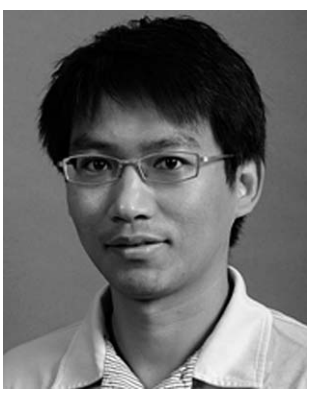

Hui-Chuan Cheng

Hui-Chuan Cheng is currently working toward the Ph.D. degree at the College of Optics and Photonics, University of Central Florida. He is a recipient of 2011 SID distinguished student paper award. His current research interests include blue phase LCDs, sunlight readable LCDs, and touch panels.

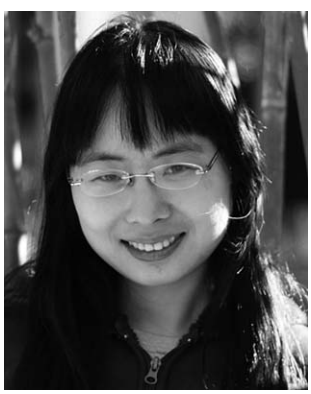

Yan Li

Yan Li is a fourth year Ph.D. student at the College of Optics and Photonics, University of Central Florida. She is a recipient of 2011 SID distinguished student paper award, 2009 J. SID outstanding student paper of the year award, and 2009 SPIE educational scholarship. Her current research interests include energy efficient and fast response LCDs, and transflective LCDs.

Shin-Tson Wu

Shin-Tson Wu is a Pegasus professor at College of Optics and Photonics, University of Central Florida. He is a Fellow of the IEEE, OSA, SID, and SPIE, and the recipient of 2011 SID Slottow-Owaki prize, 2010 OSA Joseph Fraunhofer award/ Robert M. Burley prize, 2008 SPIE G. G. Stokes award, and 2008 SID Jan Rajchman Prize. He was the founding Editor-In-Chief of the IEEE/OSA Journal of Display Technology.

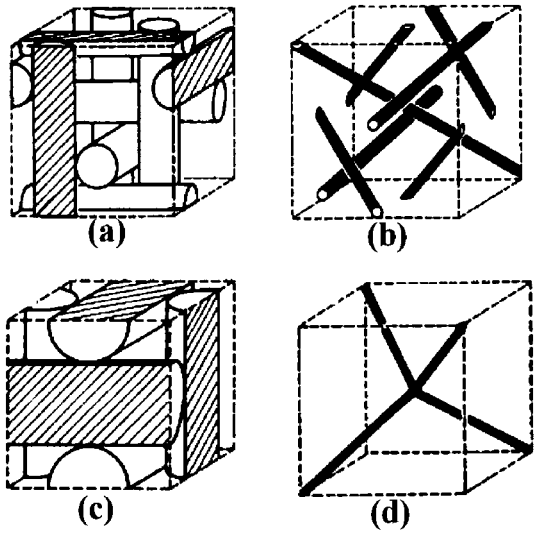

Fig. 1 Double twist cylinders in cubic structures of BPI [(a) and (b)] and BPII [(c) and (d)]. The black lines in (b) and (d) represent defect lines for the structure.

lattice distortion in the range of tens of millisecond,[12] and phase transition a few seconds.[15]

For a PSBP, the electrostriction and phase transition effects can be ignored since the lattice distortion will cause a shift in the reflected wavelength, which was not observed in the polymer stabilized system.[9] Therefore, the submillisecond response time of PSBP originates from the Kerr effect.

In the voltage-off state, a polymer-stabilized BPLC is optically isotropic. Its refractive index can be written as:[16]

$$n_{iso} = \sqrt{\left(2n_o^2 + n_e^2\right)/3}, \tag{2}$$

where n_o and n_e are the ordinary and extraordinary refractive indices of the LC composite, respectively. When the birefringence ($n_e - n_o$) is small, eqn (2) can be approximated by:

$$n_{iso} \approx (2n_o + n_e)/3. \tag{3}$$

When an electric field is applied, birefringence is induced. The optic axis of the induced refractive-index ellipsoid is along the electric field direction. As described above, the induced birefringence is due to the local reorientation of the molecules in a PS-BPLC; therefore, it is quite reasonable to assume that the average refractive index keeps constant at any electric field, which was later validated experimentally:[17]

$$n_{\text{average}} = \frac{2n_o(E) + n_e(E)}{3} = n_{iso}. \tag{4}$$

Here, $n_o(E)$ and $n_e(E)$ are the field dependent refractive index perpendicular and parallel to the electric field, respectively. With eqn (3) and (4), the ordinary refractive index change under an electric field can be expressed as:

$$\delta n = n_{iso} - n_o(E) = \frac{n_e(E) - n_o(E)}{3} = \frac{\Delta n_{ind}}{3}. \tag{5}$$

This ordinary refractive index change can be measured by a Michelson interferometer.[18] The PS-BPLC employed in this study is a mixture consisting of nematic LC (49 wt% Merck BL038), chiral dopants (21% Merck CB15 and 6% ZLI-4572) and monomers (9% EHA and 15% RM257). The BPLC was sandwiched between two ITO (indium-tin-oxide) glass substrates with a cell gap of 8 μm. Fig. 2 depicts the measured refractive index change (δn) of a PSBP cell under different driving voltages. It was observed that δn is linearly proportional to E^2 in the weak field region, as expected from Kerr effect. As the electric field increases, the induced refractive index change (δn) gradually saturates.

To explain the saturation trend of the experimental data, the following exponential convergence model, called the extended Kerr effect, was proposed and the fitting with the experimental data was quite good, as shown in Fig. 2.

$$\delta n = \delta n_{sat}\left(1 - \exp\left[-\left(\frac{E}{E_s}\right)^2\right]\right), \tag{6}$$

here δn_{sat} stands for the saturated ordinary refractive index change and E_s represents the saturation field.

The parameters obtained through fitting are $\delta n_{sat} = 0.038$ and $E_s = 13.9$ V μm^{-1}. The employed LC host has an intrinsic birefringence of 0.272. Taking into account the LC concentration (~50%) and the factor of 1/3 shown in eqn (5), the obtained refractive index change is still ~18% smaller than the ideal value, which is 0.045. This difference could be attributed to following two factors: 1) a portion of LC is embedded in the polymer network so that they do not respond to the electric field; and 2) the relatively low clearing temperature (~60 °C) of the PS-BPLC so that the order parameter at the room temperature (~23 °C) is reduced accordingly.

The Taylor expansion of eqn (6) leads to Kerr effect under weak field approximation. The Kerr constant can be written as:

$$K = 3\delta n_{sat}/(\lambda E_s^2) = \Delta n_{sat}/(\lambda E_s^2) \tag{7}$$

where Δn_{sat} is the saturated induced birefringence. With the obtained fitting values of δn_{sat} and E_s, the Kerr constant for the employed material was calculated from eqn (7), which is ~1 nm V^{-2}.

For display applications using IPS electrodes, transverse electric fields are generated and phase retardation accumulated along the beam path. However, in an IPS cell the electric field is not uniform. In 2009, a simulation model[19,20] was developed to describe the electro-optic performance of an IPS cell, taking the nonuniform electric field into consideration. With the development of the extended Kerr effect, which was incorporated into the simulation program, the performance of PS-BPLC display can be calculated more accurately.

3. Wavelength effect

Besides the saturation phenomenon under high electric field, another confusion that may be caused by eqn (1) is the wavelength dependency of the induced birefringence. Will the induced birefringence increase with the wavelength because K is called a "constant"? To investigate the dispersion relation of the optically isotropic LC material,[21] a PSIP LC composite was prepared consisting of 56 wt% nematic LC host MLC-14200, 29 wt% chiral dopants (24% CB15 and 5% ZLI-4572, Merck) and 15 wt%

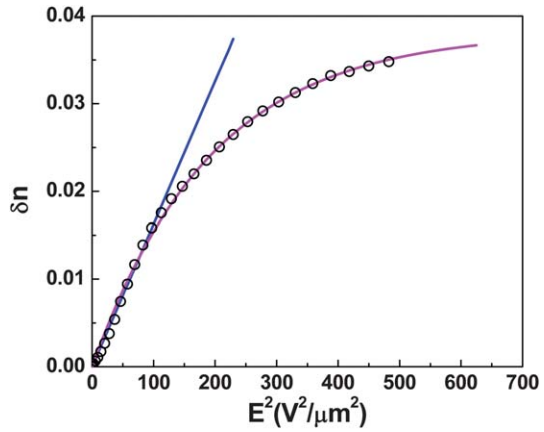

Fig. 2 Measured refractive index change (circles) and fittings with Kerr effect (straight line) and extended Kerr effect (curve).

monomers (6% RM-257 and 9% EHA). The LC/monomer mixture was injected to an IPS cell with electrode width ~10 μm, electrode gap ~10 μm, and cell gap ~7.5 μm. The cell was then cured by a UV lamp (λ ~ 365 nm) at 70 °C, which was well above the isotropic temperature of the LC/monomer mixture. In the optical setup, white light source and five color filters with transmission peaks at λ ~ 450 nm, 500 nm, 550 nm, 633 nm and 660 nm and bandwidth ~±5 nm were employed. The LC cell was sandwiched between two crossed polarizers with the striped electrodes oriented at 45° with respect to the polarizer's transmission axis. The corresponding voltage-dependent transmittance (VT) curves were measured at room temperature (~23 °C) under different wavelengths.

Fig. 3 shows the measured VT curves of the LC composite at five wavelengths. From left to right, the corresponding wavelengths are 450 nm, 500 nm, 550 nm, 633 nm and 660 nm. Because the luminous flux of each wavelength is different, the transmittance at each wavelength was normalized to its own peak value. The operating voltage is lower at a shorter wavelength for two reasons: 1) the induced phase retardation is inversely proportional to the wavelength, thus a shorter wavelength will exhibit a larger phase retardation under the same driving voltage; 2) the induced birefringence decreases with wavelength under normal dispersion condition. Considering these two factors, the required operating voltage is lower for a shorter wavelength.

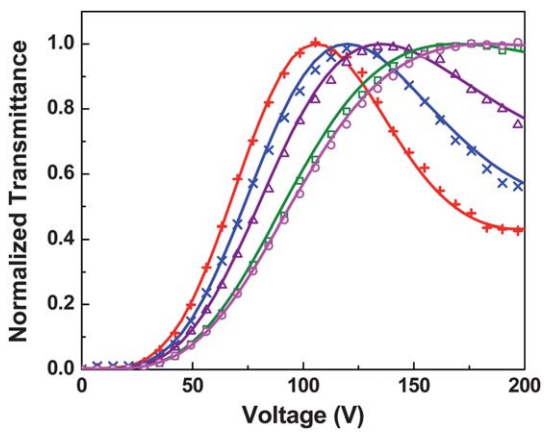

Fig. 3 Measured (dots) and fitted (lines) VT curves of the PSIP LC cell at different wavelengths. From left to right, the corresponding wavelengths are 450 nm, 500 nm, 550 nm, 633 nm and 660 nm.

Simulation with the extended Kerr effect was carried out to fit the experimental data. Since the electric field distribution is non-uniform, the local induced birefringence was calculated based on the electric field distribution. Later, an extended Jones Matrix method[22,23] was employed to calculate the averaged transmittance. The fitting results are shown in Fig. 3, in which dots represent experimental data and curves are fitting results. They overlap with each other very well at each wavelength. There are two fitting parameters: Δn_{sat} and E_s. These fitting parameters at each wavelength are listed in Table 1.

It is interesting to note that the fitting parameter E_s remains the same for all the wavelengths studied. Because at a given temperature and voltage the LC director reorientation profile is determined by the balance between elastic and electric torques, and the LC director distribution will not be affected by the probing wavelength. However, the VT curves will be different for a different wavelength because Δn_{sat} does depend on the wavelength, as shown in Table 1. Moreover, the phase retardation is a term varying with wavelength.

The wavelength dependent Δn_{sat} for the PSIP LC composite is shown in the lower trace of Fig. 4, in which dots stand for the experimental data listed in Table 1 and solid line represents the fitting curve with following single-band birefringence dispersion model:[24,25]

$$\Delta n_{sat} = G\frac{\lambda^2\lambda^{*2}}{\lambda^2 - \lambda^{*2}} \xrightarrow{\lambda \gg \lambda^*} G\lambda^{*2}, \quad (8)$$

where λ^* is the resonant wavelength of the LC composite and G is a proportionality constant. For a conjugated LC compound, the two $\pi \rightarrow \pi^*$ electronic transitions which corresponds to the resonant wavelength usually occur in the UV region.[26] Similar to nematic LCs, the dispersion of PSIP LC composite also follows the single-band birefringence dispersion model well. Through fittings, it was found that $\lambda^* \sim 216$ nm and $G \sim 1.205 \times 10^{-6}$ nm^{-2}.

To correlate the dispersion property between the PSIP composite and the LC host, we also measured the birefringence dispersion of the LC host (MLC-14200) using an Abbe refractometer. The measured data are included in the upper part of Fig. 4 where the solid line is the fitting curve based on eqn (8) with $\lambda^* \sim 218$ nm and $G \sim 3.047 \times 10^{-6}$ nm^{-2}. The two obtained λ^* values agree with each other within 1%. This is not surprising because the dispersion of the PSIP LC composite is primarily

Table 1 Fitting results of the saturated induced birefringence (Δn_{sat}), saturation electric field (E_s), and Kerr constant of the PSIP LC composite at the corresponding wavelength

λ (nm)	Δn_{sat}	E_s (V μm^{-1})	K (nm V^{-2})
450	0.0730	6.8	3.51
500	0.0695	6.8	3.01
550	0.0670	6.8	2.63
633	0.0635	6.8	2.17
660	0.0630	6.8	2.06

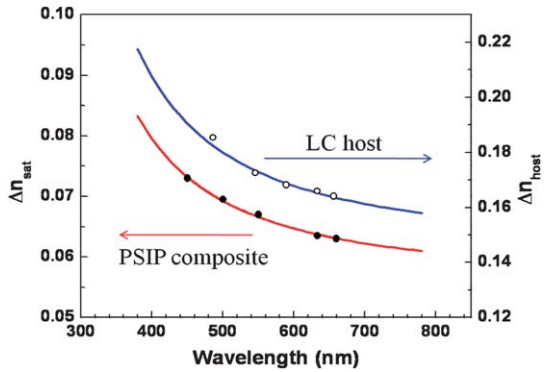

Fig. 4 Dispersion relations of the saturated induced birefringence of the PSIP LC composite (filled circles) and its nematic LC host MLC-14200 (open circles). Solid lines are fitting curves.

determined by the LC host employed. On the other hand, the decreased G value of the polymer-stabilized optically isotropic LC composite mainly originates from the decreased LC concentration. In the PSIP LC composite, the LC concentration is only ~56 wt% and the rest are chiral dopants and photocurable monomers. Thus, the expected decrease in birefringence is ~44%, but the obtained G value is decreased by ~60%. This excessive ~16% reduction could be attributed to two unaccounted factors: 1) the LC composite has a lower clearing temperature than its host, and 2) some LC molecules could be trapped by the polymer networks during polymerization process. The lower clearing point leads to a lower order parameter while the trapped LC molecules are hardly reoriented by the applied electric field.

From Fig. 4, Δn_{sat} of the PSIP LC composite decreases as the wavelength increases. When the wavelength is much longer than the resonant wavelength λ^*, the induced birefringence gradually saturates to a plateau ($G\lambda^{*2}$) according to eqn (8). When a PSIP LC composite is used in the infrared region (say, $\lambda > 1$ μm), the induced birefringence will reach a saturation level, similar to nematic liquid crystals.

Under the low field approximation, the extended Kerr effect is reduced to the conventional Kerr effect. Kerr constants were calculated from eqn (7). As shown in Table 1, the obtained Kerr constant decreases gradually with wavelength. Based on eqn (7) and (8), a dispersion relation of Kerr constant is derived as follows:

$$K = \frac{G\lambda^2\lambda^{*2}}{E_s^2\left(\lambda^2 - \lambda^{*2}\right)} = \frac{A\lambda^2\lambda^{*2}}{\lambda^2 - \lambda^{*2}} \tag{9}$$

where $A = G/E_s^2$ is a proportionality constant. In Fig. 5, the Kerr constant data are fitted with eqn (9) using $\lambda^* \sim 216$ nm and $A \sim 0.0262$ nm^{-1}. The well-fitted results clearly indicate the implicit wavelength dependency of Kerr constant.

4. Temperature effect

Since the Kerr constant plays a crucial role on the performance of an optically isotropic LC composite, the temperature dependency of the Kerr constant was investigated recently.[27] Similar to the abovementioned wavelength effect, an IPS cell with PSIP material was prepared and VT curves were measured with a CW He–Cd laser ($\lambda = 441.8$ nm) under different temperatures.

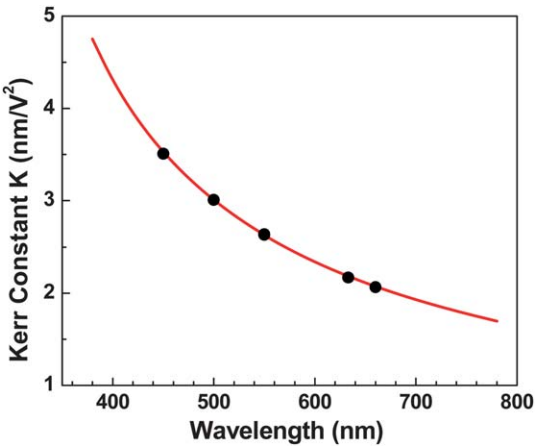

Fig. 5 Measured Kerr constant (circles) and the fitting results (solid line) of the PSIP LC composite at different wavelengths.

Fig. 6 shows the normalized VT curves measured from 15 °C to 37.5 °C (where the total phase retardation is still larger than 1π). As the temperature increases, the on-state voltage (V_{on}; corresponding to the peak transmittance) shifts rightwards, indicating that Kerr constant decreases with the temperature. These VT curves were fitted with the extended Kerr effect model [eqn (6)] at each temperature. The obtained K values (calculated from eqn (7)) are plotted in Fig. 7. As the temperature increases, the Kerr constant decreases gradually.

To explain this trend quantitatively, the temperature dependent Kerr constant needs to be derived. It has been reported by Gerber that the Kerr constant can be approximated by the following equation:[28]

$$K \sim \frac{\Delta n_{ind}}{\lambda E^2} \approx \Delta n \cdot \Delta\varepsilon \frac{\varepsilon_o P^2}{k\lambda(2\pi)^2}. \tag{10}$$

where Δn_{ind} is the induced birefringence, Δn, $\Delta\varepsilon$ and k are the intrinsic birefringence, dielectric anisotropy, and elastic constant of the host LC material, and P is the pitch length. Furthermore, it is known that Δn, $\Delta\varepsilon$ and k are related to the nematic order parameter (S) as $\Delta n \sim \Delta n_o S$,[24] $\Delta\varepsilon \sim S/T$, $k \sim S^2$.[29] The pitch length can be treated as temperature independent for a PS-BPLC, since the reflected color does not change noticeably with the temperature. This assumption should also be valid for the PSIP.

Substituting these parameters into eqn (10), we derive the temperature dependent Kerr constant as following:

$$K \approx \Delta n \cdot \Delta\varepsilon \frac{\varepsilon_o P^2}{k\lambda(2\pi)^2} \sim \Delta n_o S \cdot \frac{S}{T} \cdot \frac{1}{S^2} \cdot \frac{\varepsilon_o P^2}{\lambda(2\pi)^2} \sim \alpha \cdot \frac{1}{T}. \tag{11}$$

From eqn (11), the Kerr constant is linearly proportional to the reciprocal temperature, and α is the proportionality constant. However, as the temperature approaches the clearing point (T_c) of the LC composite, the Kerr constant should vanish (or at least decreased dramatically) because both Δn and $\Delta\varepsilon \rightarrow 0$. To satisfy this boundary condition, eqn (11) is rewritten as follows:

$$K = \alpha \cdot \left(\frac{1}{T} - \frac{1}{T_c}\right). \tag{12}$$

Eqn (12) predicts that Kerr constant decreases linearly with reciprocal temperature ($1/T$) and eventually vanishes as the temperature reaches the clearing point of the LC composite.

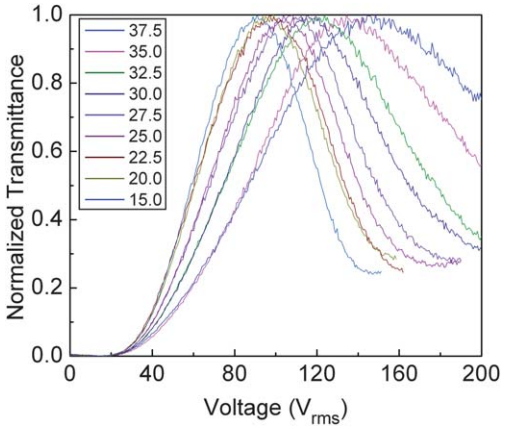

Fig. 6 Voltage dependent normalized transmittance curves of the PSIP LC cell measured from 15 °C to 37.5 °C. Electrode width = 10μm, electrode gap = 10μm, and cell gap = 7.5 μm. $\lambda = 441.8$ nm.

The Kerr constants obtained were fitted with eqn (12) while the linear coefficient α and clearing temperature T_c were set as adjustable parameters. Results are depicted in Fig. 7. From fittings, it was found that $\alpha = 1.08 \times 10^{-5}$ $m{\cdot}K/V^2$ and $T_c = 327.58$ K (54.43 °C). The T_c obtained matches very well with the measured clearing temperature (54 °C) of the LC composite. Thus, eqn (12) actually has only one adjustable parameter which is α.

It was also noticed in Fig. 7 that as the temperature further decreases, the Kerr constant gradually deviates from the linear extrapolation. Although the reason is not yet completely clear, the Kerr constant in the low temperature region should not increase as rapidly as the fitting line shows. In the low temperature region, the higher-order term of the elastic constant should be taken into consideration.[27]

Through fitting the VT curves shown in Fig. 6, the obtained Δn_{sat} under different temperatures were plotted in Fig. 8. As the temperature increases, Δn_{sat} decreases gradually. The temperature dependent Δn_{sat} is proportional to the order parameter (S) which in turn can be approximated by Haller's semi-empirical equation:[30]

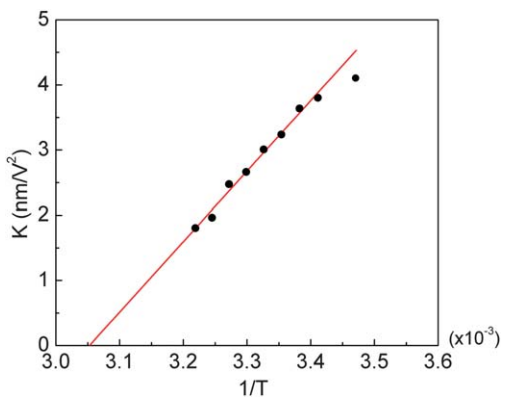

Fig. 7 Linear fit of the Kerr constant with the reciprocal temperature according to eqn (12). T: Kelvin temperature. The fitting parameter is $\alpha = 1.08 \times 10^{-5} m{\cdot}K/V^2$.

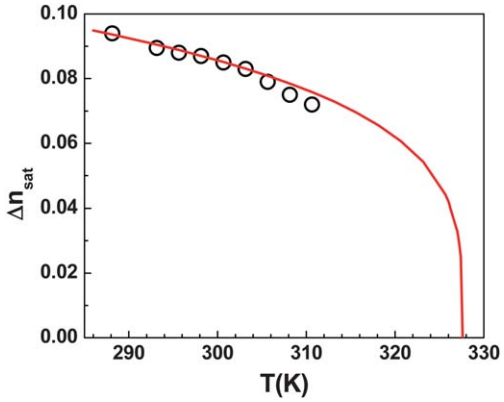

Fig. 8 Temperature dependent saturated induced birefringence. Open circles are experimental data and line represents fitting using eqn (11) with $(\Delta n_s)_o = 0.159$ and $\beta = 0.25$.

$$\Delta n_{sat} = (\Delta n_s)_o S, \tag{13}$$

and

$$S = (1 - T/T_c)^{\beta}. \tag{14}$$

where $(\Delta n_s)_o$ is the extrapolated birefringence at $T = 0$ K, T_c is the clearing temperature of our LC composite (~54 °C), and the exponent β is a material constant. For nematic LC materials, β is ~0.21 ± 0.06.[31,32] Eqn (14) works well as long as the temperature is not too close (within 1 °C) to the clearing point. As shown in eqn (13) and (14), there are two fitting parameters: $(\Delta n_s)_o$ and β. From the fitting curve shown in Fig. 8, we found $(\Delta n_s)_o = 0.159$ and $\beta = 0.25$. For comparison, the temperature dependent birefringence of our nematic host was also measured and $(\Delta n_s)_{o\text{-}host} = 0.275$, $\beta_{host} = 0.245$. The material constant β of the PSIP composite keeps almost the same as that of the host LC material, which means that the polymer only helps to stabilize the molecular arrangement in the LC composite but does not affect the intrinsic material property of the host LC noticeably. On the other hand, knowing $(\Delta n_s)_{o\text{-}host} = 0.275$ and LC concentration (~54.8%) in our LC/polymer composite we estimate that $(\Delta n_s)_o \sim 0.151$, which is quite similar to the value ($(\Delta n_s)_o = 0.159$) obtained through fitting. The difference is less than 5%. Good agreement between our experimental results and physical models was thus obtained.

Fast response time is one of the most attractive features of blue-phase (or optically isotropic) LCDs since it helps to reduce motion blur and enable color-sequential display while minimizing color breakup. Therefore, the temperature dependent response time was also studied. Since the rise time is highly dependent on the applied voltage, only the decay time of PSIP LC composite was measured from 22.5 °C to 40 °C. The decay time is defined as 100–10% transmittance change. The measured data are plotted in Fig. 9. As the temperature increases, the decay time decreases rapidly. For example, from Fig. 9 we notice that the response time is decreased by 2× when the temperature is increased by merely 4–5 degrees. This changing rate is ~3× more sensitive than most nematic LCs.

To understand this peculiar phenomenon, a physical model was developed to explicitly correlate the temperature dependent

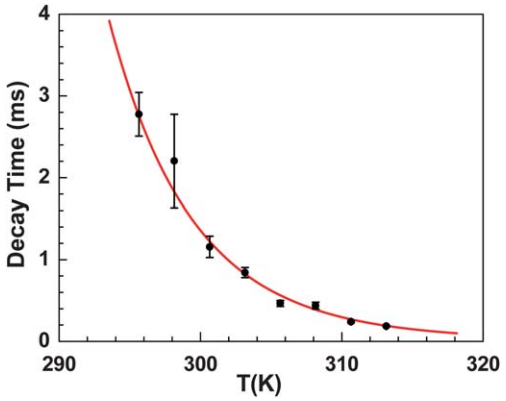

Fig. 9 Temperature dependent decay time. Dots are experimental data and line represents fitting using eqn (17) with $B = 7.16 \times 10^{-23}$ ms and $E_a = 1.31$ eV.

response time with LC parameters.[27] The free relaxation time of a polymer-stabilized blue-phase or optically isotropic LC composite can be approximated by:[15,33]

$$\tau \approx \frac{\gamma_1 P^2}{k(2\pi)^2}, \tag{15}$$

with γ_1 being the rotational viscosity, P the pitch length, and k the elastic constant. As discussed before, the pitch length is insensitive to the temperature and can be treated as a constant.

From mean field theory,[29] elastic constant is related to the nematic order parameter (S) as $k \sim S^2$. With regard to rotational viscosity, the following modified Arrhenius model works well to describe the temperature dependent rotational viscosity of nematic LCs:[34,35]

$$\gamma_1 \sim S \cdot \exp(E_a/K_B T), \tag{16}$$

where E_a is the activation energy of molecular rotation and K_B is the Boltzmann constant. With eqn (16) and treating P as a constant, eqn (15) was rewritten as:

$$\tau \approx \frac{\gamma_1 P^2}{k(2\pi)^2} \sim \frac{S \cdot \exp(E_a/K_B T) \cdot P^2}{S^2 \cdot (2\pi)^2} \approx B \cdot \frac{\exp(E_a/K_B T)}{(1 - T/T_c)^{\beta}}. \tag{17}$$

Eqn (17) has two unknowns: B and E_a. As shown in Fig. 9, eqn (17) fits quite well with the measured response time data. Through fitting, it was found $B = 7.16 \times 10^{-23}$ ms and $E_a = 1.31$ eV. The obtained activation energy is $\sim 3\times$ higher than that of E7,[36,37] which is why the response time is more sensitive to temperature. Our host nematic LC has a similar viscosity and E_a as E7. The increased E_a is believed to result from the mixed chiral dopants. From a response time viewpoint, a low viscosity host (smaller activation energy) is always favorable.

5. Remaining challenges

Although polymer-stabilized isotropic-to-anisotropic LCDs hold great potential for future display and photonic applications, some technical challenges remain to be overcome. In the first place, new materials with wider temperature range and lower driving voltage need to be developed. For display applications, the LC temperature range should cover from −40 °C to 80 °C. In a polymer-stabilized BPLC, we could choose a wide temperature range nematic LC host. However, after mixing with chiral dopant the mixture's clearing point often decreases substantially. For example, the clearing temperature of our LC host is 94 °C, but it drops to 54 °C after polymerization. This is because one of the chiral dopants employed in the PSBP mixture, which is CB15 in this specific case, has a very low clearing point (4 °C). A low clearing point PSBP will make the electro-optic properties of the LC/polymer composite, *e.g.*, VT curves and response time too sensitive to the local temperature variation of a display panel. Consequently, the requirement for better thermal uniformity of a backlight unit is increased. To avoid the dramatic decrease of clearing temperature, a chiral dopant with high twisting power and high melting point would help. However, its solubility should also be taken into consideration.

From device viewpoint, low operating voltage leads to low power consumption. The operating voltage (V_{on}) of a PSBP is governed by both device structure and material as:[27]

$$V_{on} = A/\sqrt{K}, \tag{18}$$

where A is a device parameter which is strongly dependent on the electrode configuration, and K is the Kerr constant of the PSBP material. From a materials viewpoint, polymer-stabilized BPLC represents a paradigm shift. The traditional TFT-grade nematic LCs require a modest birefringence ($\Delta n \sim 0.1$) and dielectric anisotropy ($\Delta\varepsilon \sim 5$–10), low viscosity, and high resistivity. However, to achieve a large Kerr constant ($K \sim 10$ nm V^{-2}) the BPLC should have a large $\Delta n \cdot \Delta\varepsilon$. High birefringence implies to long molecular conjugation and large dielectric anisotropy demands multiple polar groups. As a result, the viscosity of these compounds will be higher, and the tradeoff is increased response time. Recently, a BPLC with $K \sim 13.7$ nm V^{-2} at $\lambda = 633$ nm has been reported.[37] The LC host has $\Delta n \sim 0.17$ and $\Delta\varepsilon \sim 94$. Its response time at ~25 °C is around 1 ms, which is still not too bad. As the temperature increases, the response time decreases gradually.

For TFT-LCD applications, the voltage holding ratio is another crucial requirement in order to avoid image flickering. In a polymer-stabilized BPLC, two types of monomers (monofunctional and difunctional) and a small percentage of photo-initiator are used. The ionic impurities in these monomers and photo-initiator could degrade the voltage holding ratio. Therefore, better materials including LC host, monomers, and photo-initiator need to be developed, and the photo-polymerization process needs to be optimized.

In addition to developing high Kerr constant materials, device configuration also plays an important role for reducing the operating voltage as eqn (18) elucidates. Currently, the best available PSBP material has a driving voltage of 48V in an IPS cell with electrode width 10μm and electrode gap 10μm.[37] With the same material and improved device configuration such as protruded and corrugated electrode,[38–40] the driving voltage could be reduced to 10V, which enables amorphous silicon TFT driving.

Another challenge of PSBP is hysteresis. It is known that polymer-stabilized LC composites often exhibit memory effect, also known as hysteresis. Some preliminary work on the hysteresis of BPLC and polymer-stabilized BPLC has been

reported.[41] Hysteresis affects the accuracy of grayscale control and should be minimized. A side effect caused by hysteresis is the residual birefringence. After a PSBP device has been driven for many cycles, some LC molecules could not go back to their original state, which causes light leakage in the dark state and degrades the device contrast ratio.

Long term stability of PS-BPLC is another concern. The concerns of long term stability include twofold: incomplete photo-polymerization process and device operating lifetime, such as image sticking and polymer stability.

In addition to displays, BPLCs are promising candidates for photonic applications as well. They can be used in mirror-less lasing,[42,43] tunable microlens,[44,45] and photonic crystals,[46,47] just to name a few.

6. Conclusion

Tremendous progress in polymer-stabilized blue phase liquid crystals has been made recently. A record-high Kerr constant BPLC material with a reasonably high contrast ratio (>1000 : 1), fast response time (~1 ms), and low hysteresis (<6%) has been developed. New device structures with protrusion electrodes or corrugated electrodes are leading the way toward low operating voltage (<10 V) for amorphous-silicon TFT addressing. The greatly simplified fabrication process, such as no need for molecular alignment layer, and cell gap insensitivity are particularly attractive for large panel manufacturing. The fast-response feature enables color sequential displays using RGB LEDs, which in turn eliminates the spatial color filters. Consequentially, the optical efficiency and resolution density are all tripled. Low power consumption is particularly essential for energy saving, especially for large LCD panels.

There is no doubt that some technical issues remain to be addressed, *e.g.*, wider blue-phase temperature range, lower operating voltage, higher transmittance, higher contrast ratio, smaller hysteresis, and long term stability, *etc.* These problems will be gradually overcome in the near future. A big wave of next-generation display and photonic devices is emerging.

Acknowledgements

The authors are indebted to Industrial Technology Research Institute (Taiwan) and Air Force Office for Scientific Research for partial financial support under contract No. FA95550-09-1-0170.

References

1 S. A. Brazovskii and S. G. Dmitriev, *Zh. Eksp. Teor. Fiz*, 1975, **69**, 979.
2 R. M. Hornreich and S. Shtrikman, in: *Liquid Crystals of One- and Two- Dimensional Order* (edited by W. Helfrich and G. Heppke), Springer-Verlag, Berlin, 1980, p. 185.
3 S. Meiboom, J. P. Sethna, W. P. Anderson and W. F. Brinkman, *Phys. Rev. Lett.*, 1981, **46**, 1216.
4 E. Dubois-Violette and B. Pansu, *Mol. Cryst. Liq. Cryst.*, 1988, **165**, 151.
5 P. P. Crooker, in: *Chirality in Liquid Crystals*, (edited by H. S. Kitzerow and C. Bahr) Springer, New York, 2001, pp. 186–222.
6 D. L. Johnson, J. H. Flack and P. P. Crooker, *Phys. Rev. Lett.*, 1980, **45**, 641.
7 R. J. Miller and H. F. Gleeson, *Phys. Rev. E: Stat. Phys., Plasmas, Fluids, Relat. Interdiscip. Top.*, 1995, **52**, 5011.
8 H. S. Kitzerow, H. Schmid, A. Ranft, G. Heppke, R. A. M. Hikmet and J. Lub, *Liq. Cryst.*, 1993, **14**, 911.
9 H. Kikuchi, M. Yokota, Y. Hisakado, H. Yang and T. Kajiyama, *Nat. Mater.*, 2002, **1**, 64.
10 Y. Haseba, H. Kikuchi, T. Nagamura and T. Kajiyama, *Adv. Mater.*, 2005, **17**, 2311.
11 Y. Haseba and H. Kikuchi, *Mol. Cryst. Liq. Cryst.*, 2007, **470**, 1.
12 H. J. Coles and M. N. Pivnenko, *Nature*, 2005, **436**, 997.
13 K. M. Chen, S. Gauza, H. Xianyu and S. T. Wu, *J. Disp. Technol.*, 2010, **6**, 49.
14 J. Kerr, *Philos. Mag*, 1875, **50**, 337.
15 H. F. Gleeson and H. J. Coles, *Liq. Cryst.*, 1989, **5**, 917.
16 J. Li and S. T. Wu, *J. Appl. Phys.*, 2004, **95**, 896.
17 J. Yan, M. Jiao, L. Rao and S. T. Wu, *Opt. Express*, 2010, **18**, 11450.
18 J. Yan, H. C. Cheng, S. Gauza, Y. Li, M. Jiao, L. Rao and S. T. Wu, *Appl. Phys. Lett.*, 2010, **96**, 071105.
19 Z. Ge, L. Rao, S. Gauza and S. T. Wu, *J. Disp. Technol.*, 2009, **5**, 250.
20 Z. Ge, S. Gauza, M. Jiao, H. Xianyu and S. T. Wu, *Appl. Phys. Lett.*, 2009, **94**, 101104.
21 M. Jiao, J. Yan and S. T. Wu, *Phys. Rev. E*, 2011, **83**, 041706.
22 A. Lien, *Appl. Phys. Lett.*, 1990, **57**, 2767.
23 Z. Ge, X. Zhu, T. X. Wu and S. T. Wu, *J. Opt. Soc. Am. A*, 2005, **22**, 966.
24 S. T. Wu, *Phys. Rev. A: At., Mol., Opt. Phys.*, 1986, **33**, 1270.
25 S. T. Wu, C. S. Wu, M. Warenghem and M. Ismaili, *Opt. Eng.*, 1993, **32**, 1775.
26 S. T. Wu, E. Ramos and U. Finkenzeller, *J. Appl. Phys.*, 1990, **68**, 78.
27 L. Rao, J. Yan and S. T. Wu, *J. Soc. Inf. Disp.*, 2010, **18**, 954.
28 P. R. Gerber, *Mol. Cryst. Liq. Cryst.*, 1985, **116**, 197.
29 W. Maier and A. Saupe, *Z. Naturforsch, Teil A*, 1960, **15**, 287.
30 I. Haller, *Prog. Solid State Chem.*, 1975, **10**, 103.
31 S. T. Wu, A. M. Lackner and U. Efron, *Appl. Opt.*, 1987, **26**, 3441.
32 J. Li, S. Gauza and S. T. Wu, *J. Appl. Phys.*, 2004, **96**, 19.
33 D. K. Yang and S. T. Wu, *Fundamentals of Liquid Crystal Devices*, Wiley, 2006.
34 S. T. Wu and C. S. Wu, *Liq. Cryst.*, 1990, **8**, 171.
35 S. T. Wu and C. S. Wu, *Phys. Rev. A: At., Mol., Opt. Phys.*, 1990, **42**, 2219.
36 M. Schadt and F. Muller, *IEEE Trans. Electron Devices*, 1978, **25**, 1125.
37 L. Rao, J. Yan, S. T. Wu, S. Yamamoto and Y. Haseba, *Appl. Phys. Lett.*, 2011, **98**, 081109.
38 L. Rao, Z. Ge, S. T. Wu and S. H. Lee, *Appl. Phys. Lett.*, 2009, **95**, 231101.
39 M. Jiao, Y. Li and S. T. Wu, *Appl. Phys. Lett.*, 2010, **96**, 011102.
40 S. Yoon, M. Kim, M. S. Kim, B. G. Kang, M. K. Kim, A. K. Srivastava, S. H. Lee, Z. Ge, L. Rao, S. Gauza and S. T. Wu, *Liq. Cryst.*, 2010, **37**, 201.
41 K. M. Chen, S. Gauza, H. Xianyu and S. T. Wu, *J. Disp. Technol.*, 2010, **6**, 318.
42 W. Cao, P. Palffy-Muhoray and B. Taheri, *Nat. Mater.*, 2002, **1**, 111.
43 S. Yokoyama, S. Mashiko, H. Kikuchi, K. Uchida and T. Nagamura, *Adv. Mater.*, 2006, **18**, 48.
44 Y. H. Lin, H. S. Chen, H. C. Lin, Y. S. Tsou, H. K. Hsu and W. Y. Li, *Appl. Phys. Lett.*, 2010, **96**, 113505.
45 C. H. Lin, Y. Y. Wang and C. W. Hsieh, *Opt. Lett.*, 2011, **36**, 502.
46 P. Etchegoin, *Phys. Rev. E: Stat. Phys., Plasmas, Fluids, Relat. Interdiscip. Top.*, 2000, **62**, 1435.
47 M. Thiel, M. S. Rill, G. von Freymann and M. Wegener, *Adv. Mater.*, 2009, **21**, 1.